International Journal of Scientific Engineering and Applied Science (IJSEAS) – Volume-7, Issue-5, May 2021
ISSN: 2395-3470
www.ijseas.com

A Numerical Study of Ranque-Hilsch Vortex Tube

Kamel A. Elshorbagy[1], Baher A. Aboulkoll[2]*

[1] Professor, Alexandria University, Faculty of Engineering, Mech. Eng. Dept., Alexandria, 21544

[2] Research Assistant, Alexandria University, Faculty of Engineering, Mech. Eng. Dept., Alexandria, 21544

* Corresponding Author, E-mail: baher.aboulkoll@gmail.com

Abstract The Ranque-Hilsch Vortex Tube (RHVT) tube is a simple device used in industry for generation of cold and hot air streams from a single compressed air supply. A numerical study of the tube is introduced here using 2D axisymmetric with swirl, k-ε turbulence model computed by ANSYS Fluent® software package whose results shows promising agreement with the experimental measurements.

The objective of this paper is the demonstration of the successful use of CFD in providing a tool that can be used to optimize vortex tube design as well as assess its performance.

Keywords Ranque Hilsch, Vortex tube, RHVT

Nomenclature

A	Area, (mm^2)
c_p	Constant pressure specific heat capacity of air at room temperature, (kJ kg^{-1} K^{-1})
$\dot{m}$	Mass flow rate, (kg s^{-1})
$\dot{Q}$	Power separation (kW)
T	Temperature (K)
V	Velocity (m s^{-1})

Greek Letters

θ	Nozzle angle

Subscripts

c	Cold stream
h	Hot stream
in	Inlet
m	Model
n	Normal
r	Radial
θ	Tangential

Introduction

The vortex tube is a device without moving mechanical parts, which converts a flow of compressed gas, initially homogeneous in temperature, into two separate flows, one of a low total temperature and the other of a high one. Such a separation of the flow into two temperature regimes is termed as the Temperature or Energy Separation Effect [1].

The vortex tube effects were first observed by Ranque, a French metallurgist and physicist about 1930. He formed a small company to exploit the item but it soon failed. He presented a paper on the vortex tube to a scientific society in France in 1933, but it was met with disbelief and disinterest. Thereafter, the vortex tube disappeared for several years, until Rudolph Hilsch studied it and published his findings in the mid-1940s [2].
In 1947, Hilsch systematically examined the effect of the inlet pressure and the geometrical parameters of the vortex tube on its performance and presented a possible explanation of the energy separation process [2].

The vortex tube has several types but the most common one that normally used for commercial purposes is counter-flow vortex tube. In this type, the vortex tube contains the following parts: one or more inlet nozzles, a vortex generator, a cold and hot end orifice in opposite direction, a hot end control valve and a tube [3] as shown in “Fig.1.”.

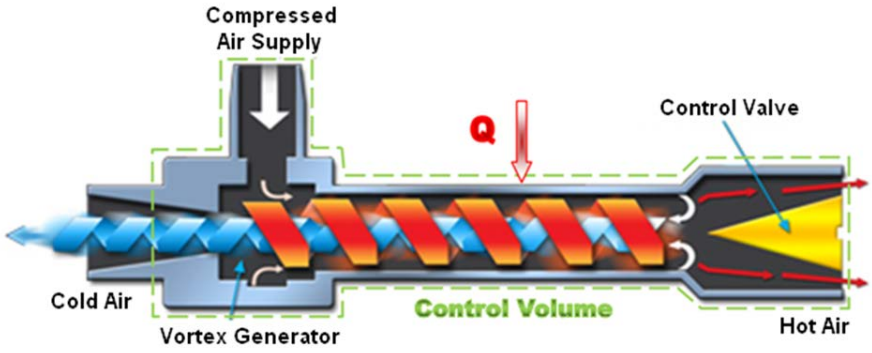

Figure 1: Cross section of Ranque-Hilsch Vortex Tube [4]

Ranque proposed that compression and expansion effects are the main reasons for the temperature separation in the tube. He noticed that the air entering tangentially into a pipe exits from one outlet at a lower temperature and from the other outlet at a higher temperature than the inlet flow temperature [5,6]. Later, the geometrical parameters and performance optimization of the tube were investigated by Hilsch. He added the effect of inner friction to the Ranque’s model of compression and expansion by studying the Ranque’s findings and performed experimental and theoretical studies on the vortex tube gas flow to improve its efficiency. He worked on spiral flow using smoke visualization inside a vortex tube in which inner wall is covered by oil. So, Ranque-Hilsch vortex tube named after them. [5,6].

The fluid which rotates in a vortex along the axis may touch the high speed up to 1,000,000 RPM. And due to this Vortex tubes are able to generate temperatures down to 100°F below inlet air temperature [7].

Even though a significant interest has been created by these applications, the physical phenomenon responsible for the temperature separation is still being debated. One of the obstacles to investigations of RHVT is the lack of substantial published literature review. An important aspect of any research work on RHVT should be to collect together a significant mass of published literature [8].

Many experimental studies have been carried on RHVT, however, very few of them have been able to predict profiles of pressure, temperature and velocity vectors inside RHVT. After the advent of modern digital high-speed computation facilities, a number of Computational Fluid Dynamics (CFD) studies have been carried out to understand the physics of RHVT [9].

They are widely used for commercial low temperature applications such as cooling of electrical parts, cutting tools and testing of thermal sensors and local heating of enclosures [10].

There are recent efforts to use them in fast starting up of the steam power plants, liquefying natural gas, separating mixed gases and providing cooled special environments in the laboratories [11,12].

Working Principle

The energy separation occurred in the RHVT between the cold and hot streams creates the temperature difference between the inlet and outlet streams [13]. Several researchers investigated the phenomena of energy separation in vortex tube then suggested various theories to explain it [13,14].

Sahu, et al. [15] suggested that the highly compressed air is forcing through a generation chamber, and by the virtue of high pressure and limited volume the pressure head of feeding air is get converted into the kinetic head which generates the centrifugal spin of air along the inner walls of the tube. pressurized gas is injected tangentially into a swirl chamber and accelerates to a high rate of rotations.
The Compressed air which is supplied to the vortex tube and passes through nozzles that are tangent to an internal counter bore. These nozzles set the air in a vortex motion similar to tornado [15].
The remainder of the gas is forced to return in an inner vortex of reduced diameter within the outer vortex. A percentage of the hot, high-speed air is permitted to exit at the control valve. The remainder of the (now slower) air stream is forced to counter flow up through the center of the high-speed air stream, giving up heat, through the center of the generation chamber finally exiting through the opposite end as extremely cold air [15].

Maheswaran A et al. [16] proposed that the angular velocity of inner vortex and outer vortex are same. But according to the law of conservation of angular momentum the velocity of

inner vortex expected to be increase but the velocity of inner vortex remains the same. Thus, the angular momentum has been lost from inner vortex.
This lost energy is shown as heat in the outer vortex. Thus, the outer vortex become heat and the inner vortex is cold in the vortex tube. Thus, the outer vortex become heat and the inner vortex is cold in the vortex tube, the fluid enters the tube along the periphery of the tube and setup a swirling flow which sets up a centrifugal field and a pressure gradient. Centrifugal field is responsible for air to flow in vortex motion along the periphery of the tube [16].
Because of the high flow speed requires to set up centrifugal filed, fluid friction results in significant viscous dissipation at the periphery, that is heating, which must be removed. The flow is driven from the periphery to the center of tube by a pressure gradient that opposes the centrifugal field induced by rotation. When the flow overcomes the centrifugal field by pressure gradient, gas expands and obtain a lower temperature and comes out through cold end [16].

Kurosaka [17] attempted to explain the energy separation inside the VT by acoustic streaming. He proposed that the energy separation is due to damping of acoustic streaming.

The effect of friction and turbulence inside the VT has always been a major concern of many researchers and was considered by some researchers as the reason for energy separation. For example, using a simple vortex tube model with CFX software and k-ε turbulence model, Kazantseva et al. [18] attributed the energy separation inside the VT to the energy and gas dynamic interaction of vortices inside the VT.

Another studies [13,14], using a simple vortex tube model with CFD software and k-ε turbulence model to computationally investigate the different effects on the performance of the RHVT.

Experimental Data

The current CFD model is validated by comparing its results with the experimental measurements of Skye et al. [14]. An Exairw 708 slpm (25 scfm) vortex tube was used in their research to collect all of the experimental data reported; the raw data can be found in Skye [19]. The vortex tube was energized with compressed air at a nominal inlet gauge pressure of 483 kPa (70 psig). The valve that typically controls the hot exit pressure of the vortex tube was removed; instead, a valve on the rotameter located downstream of the hot exit was used to control the hot exit pressure in order to facilitate the measurement of the pressure. A schematic of the setup and list of equipment is shown in in “Fig.2.”.

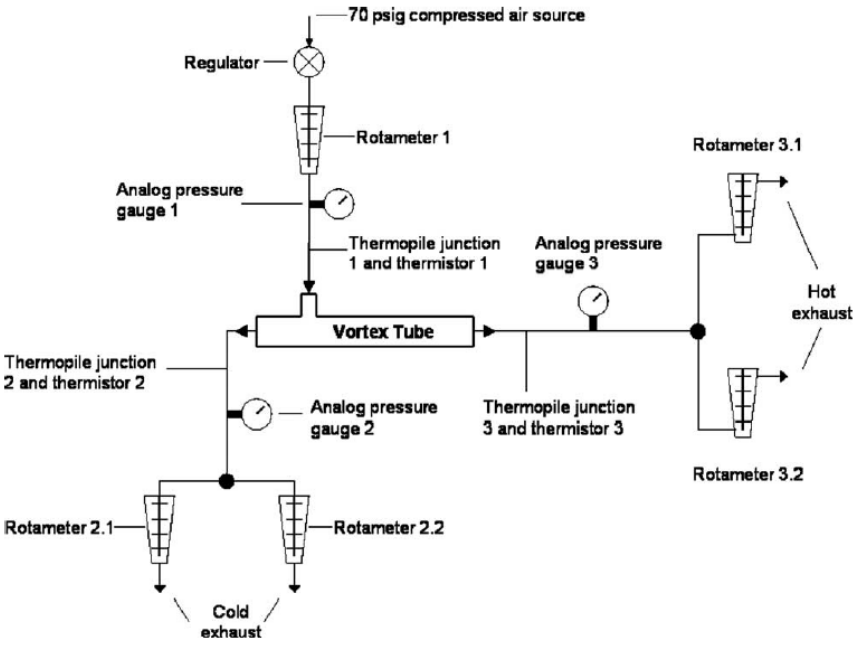

Figure 2: Schematic of the experimental setup [14]

Measurements of the volume flow rate were taken immediately before the inlet and at both exits of the vortex tube using variable area rotameters [14]. The rotameters that measured the flow leaving the vortex tube were vented to atmosphere and therefore atmospheric pressure (measured using a barometer) was used to determine the actual density at these locations. The density and volumetric flow rate together were used to obtain the mass flow rate ($\dot{m}$) associated with each of the respective streams [14].

Pressure measurements were taken using analog pressure gauges. The absolute values of the inlet and exit temperatures were measured with thermistors that were inserted into the fluid stream [14].

The power separation that is induced in the hot and cold streams that exit the vortex tube ($\dot{Q}_h$and $\dot{Q}_c$, respectively) are given by the following equations:

$$\dot{Q}_h = \dot{m}_h\, c_p (T_h - T_{in}) \quad (1)$$

$$\dot{Q}_c = \dot{m}_c\, c_p (T_{in} - T_c) \quad (2)$$

where $\dot{m}_h$ and $\dot{m}_c$ are the hot and cold mass flow rates, respectively, T_h, T_c, and T_{in} are the hot exit, cold exit, and inlet temperatures, respectively, and c_p is the specific heat capacity of air which is assumed to be constant and evaluated at room temperature.

Vortex Tube Geometry

The vortex tube dimensions used in CFD model are mentioned are mentioned in the Skye et al. [14] study. A picture and schematic of the vortex tube are shown in “Fig.3.”.and “Fig.4.”. The 10.6 cm working tube length is the section where the power separation occurs, and it was used as the bounding geometry for the CFD model.

The cold and hot exits are axial orifices with areas of 30.2 and 95.0 mm2, respectively [14]. The nozzle of the vortex tube consists of 6 straight slots that direct the flow to high tangential velocities. The dimensions of the nozzle were measured using digital pictures of the nozzle taken with a scale [14]

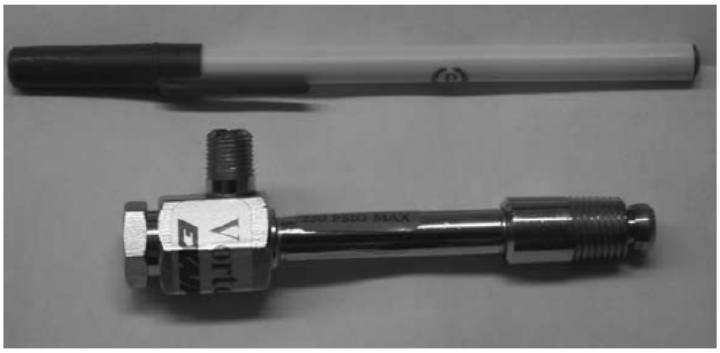

Figure 3: photo of vortex tube used in the Skye et al. experiment [14]

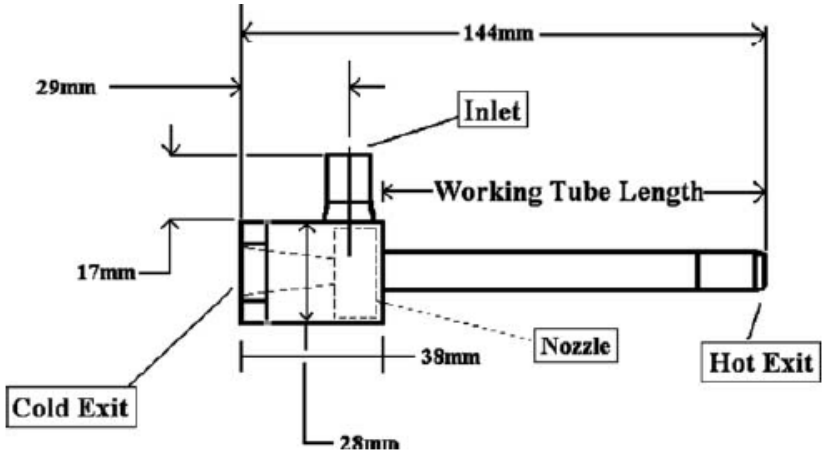

Figure 4: Schematic of vortex tube used in the Skye et al. experiment [14]

The height of each slot is 0.97 mm, the width is 1.41 mm, and the length is 3.07 mm. The total area normal to the flow (A_n) associated with six nozzles is therefore 8.15 mm2. The geometric measurements of the vortex tube are summarized in "Table 1".

Nozzle inlet vectors are defined using the convention shown in Fig. 6 where V_n represents the total velocity vector, while V_r and V_θ denote the radial and tangential components of velocity, respectively. The magnitudes of the vector components were measured using digital photographs of the Nozzle [14].

Table 1: Geometric measurements of the vortex tube [14]

Measurement	Value
Working tube length	10.6 cm
Working tube I.D.	1.14 cm
Nozzle height	0.97 mm
Nozzle width	1.41 mm
Nozzle total inlet area (A_n)	8.2 mm^2
Cold exit diameter	6.2 mm
Cold exit area	30.3 mm^2
Hot exit diameter	11.0 mm
Hot exit area	95 mm^2
L1	2.08
L2	0.54
Theta (Y)	75.48
Tangential velocity (V_θ)	$0.97V_n$
Radial velocity (V_r)	$0.25V_n$

CFD Model

- **General overview**

The FLUENT® software was used to create the CFD model of the working length of the vortex tube in "Fig.4.". The model is two-dimensional, axisymmetric (with swirl), steady state, and employs the standard k-epsilon turbulence model. A complete list of the model parameters can be found in Skye et al. [14,19]. The realized k-epsilon turbulence model was also investigated, but resulted not be made to converge for this simulation.

The geometric model was created using the measured dimensions [14] of the vortex tube in order to specify the length and radius, as well as the areas of the inlet and exit ports. The inlet is modeled as a continuous annular opening, which is slightly different than the 6 discrete nozzles in the experimental vortex tube.

Additionally, the CFD models the hot exit as an annular outlet, while Exair vortex tube has an axial outlet. A mesh consisting of approximately 99,000 grid points shown in "Fig. 5" was used with node concentration near the wall and boundary condition edges inlet, hot exit and cold exit. Because of the symmetry of the vortex tube, the model was defined as half of the cross section of the vortex tube as pictured in "Fig. 6".

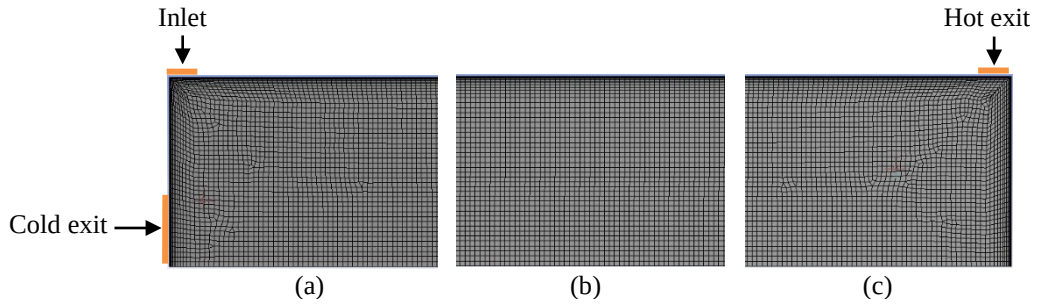

Figure 5: CFD mesh grid showing node distribution at the (a) inlet/cold exit, (b) mid-section, and (c) hot exit.

Figure 6: Schematic of the CFD model, shown with mirror image [14].

- **Grid independent study**

As shown in "Fig 7" two axial lines one in first quarter, and the other in the middle of the numerical domain which are used to evaluate the mesh independent by comparing the axial and tangential velocity components of the flow along them. Velocity radial component along the axial line is almost zero. So, it's eliminated from grid study. The simulation performed for cold fraction of 0.2 which is the ratio between $\dot{m}_c \ to \ \dot{m}_{in}$.

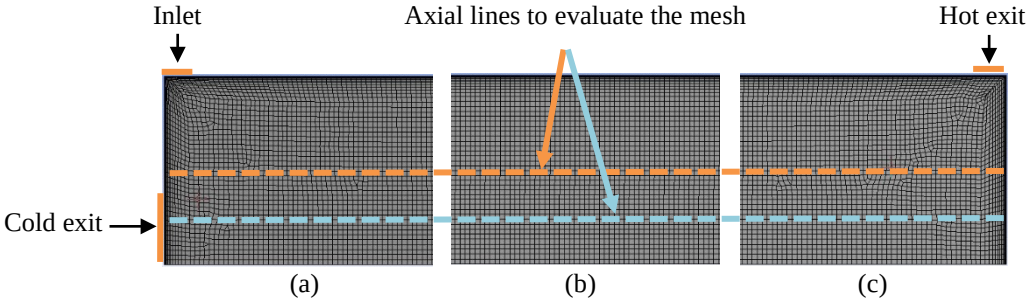

Figure 7: CFD mesh grid showing axial lines used for evaluation.

In the current study four mesh element sizes are used to evaluate grid independent as shown in grid statistics in "Fig 8". The used element mesh size between 0.00025 m and 0.00010 m generating number of elements between 14537 and 66728 elements. The selected mesh depending on comparing the velocity components distribution along the axial lines showed in "Fig 7" that will be discussed below is the third mesh of element size of 0.00015 m and number if elements of 32556.

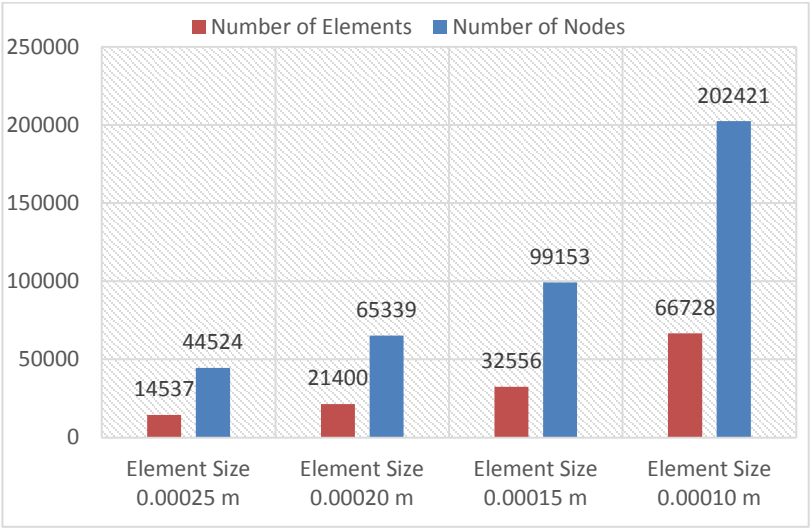

Figure 8: CFD mesh grid statistics.

The study of “Fig. 9” and “Fig. 10” which illustrate the Axial and tangential velocity components for different element sizes along the axial line in the middle of the numerical domain Shawn that the average percentage different become below 2.5% for the velocity values between mesh element size 0.00015 and 0.00010.for that the third mesh with 0.00015 m element size is preliminary selected and to confirm this by studying the velocity component along the other line in the first quarter of the numerical domain.

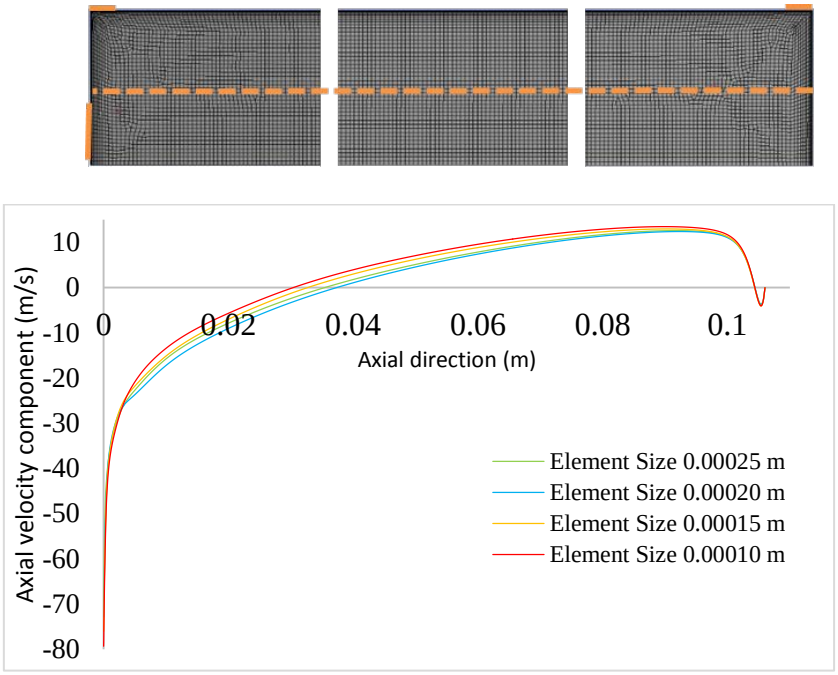

Figure 9: Axial velocity component for different element sizes along the axial line in the middle of the numerical domain.

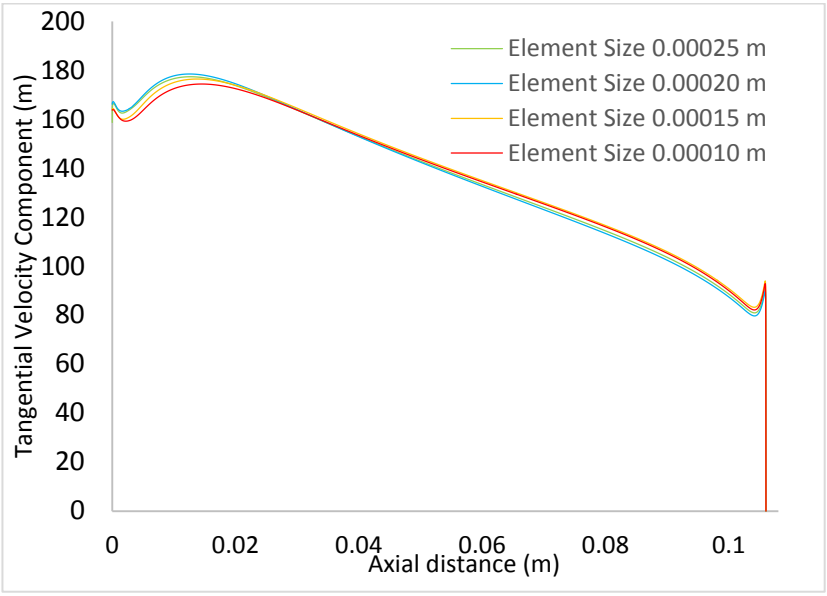

Figure 10: tangential velocity component for different element sizes along the axial line in the middle of the numerical domain.

The study of “Fig. 11” and “Fig. 12” which illustrate the Axial and tangential velocity components for different element sizes along the axial line in the first quarter of the numerical domain Shawn that the average percentage different become below 3.5% for the velocity values between mesh element size 0.00015 and 0.00010.in this case the axial values shows higher difference but the tangential ones shows lower difference. As an average for the difference for both conditions for both axial line it’s confirmed to use the mentioned before mesh element size which gives near similar values with lower than half computational time which is challenging for the current study.

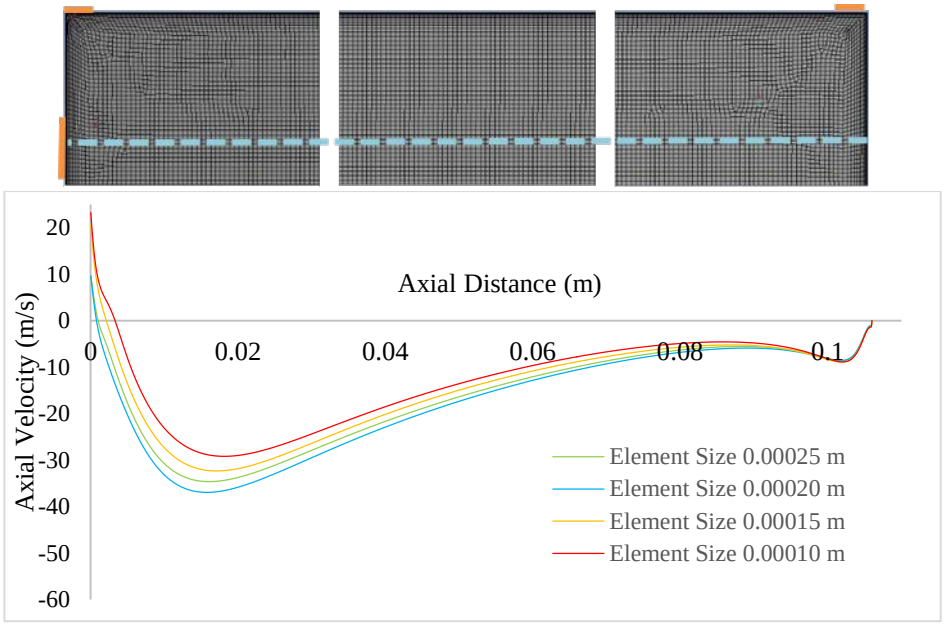

Figure 11: Axial velocity component for different element sizes along the axial line in the first quarter of the numerical domain.

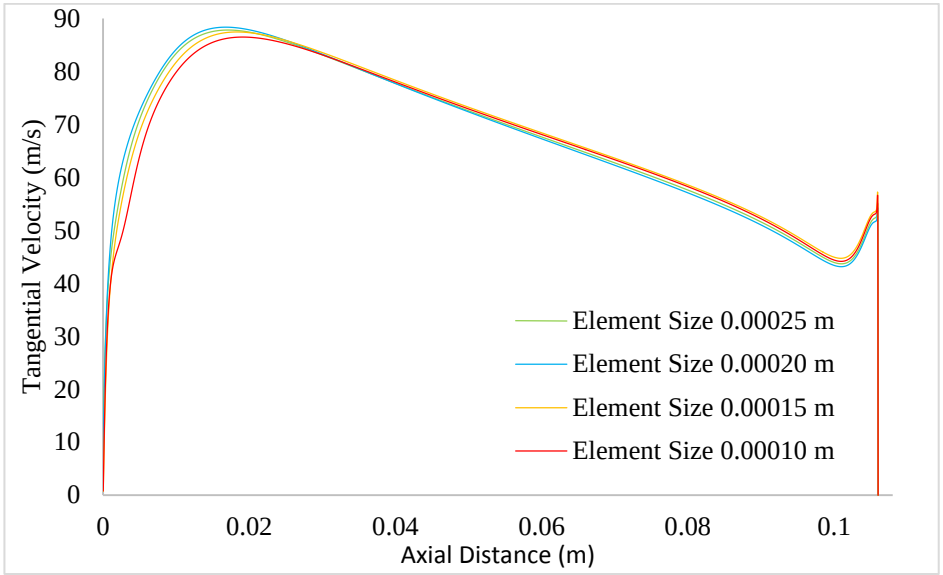

Figure 12: Tangential velocity component for different element sizes along the axial line in the first quarter of the numerical domain.

- **Boundary Conditions**

The experimental data from the study of Skye et al. [14] provided some of the boundary conditions for the inlet nozzles and both outlets while the rest of the data were acquired from different previous CFD models [13,19] which were implemented based on the experiment under consideration. The boundary conditions are summarized in "Table 2".

Table 2: Boundary conditions used in the current study [13]

Boundary condition	Type and parameter of boundary condition
Inlet nozzles	Mass flow inlet boundary condition with mass flow rate of 8.35 g/s, total temperature of 294.2 K
Cold outlet	Pressure outlet
Hot outlet	Pressure outlet
Tube wall	No slip boundary conditions with adiabatic wall
Tube axis	Axisymmetric swirl conditions for the tube axis

- **Mass flow inlet**

In the mass flow boundary conditions [13,14], a velocity is computed for each face, and this velocity is used to compute the fluxes of all relevant variables into the domain. To compute this velocity, the inputs for mass flow rate, flow direction, static pressure, and total temperature are used. The computed velocity is adjusted for each iteration so that the correct mass flow value is maintained.

For ideal gases, the static temperature and static pressure are required to compute the density. If the inlet is subsonic, the static pressure is extrapolated from the cells inside the inlet face.

The static temperature at the inlet is computed from the total enthalpy, which is determined from the input total temperature. In current case the boundary condition with mass flow rate of 8.35 g/s, total temperature of 294.2K, for velocity vector components axial velocity is zero, the radial velocity is -0.25 and tangential velocity is 0.975.

For turbulence specification method used intensity and hydraulic diameter.

- **Pressure outlet**

In the pressure outlet boundary conditions [13,14], the face pressure at the boundary is same as the value specified in the dialog box. For subsonic flow, the pressure at the faces of the outlet boundary is computed using a weighted average of the left and right state of the face boundary. This weighting is a blend of fifth-order polynomials.

The exit pressure is not constant along the pressure outlet boundary. However, upon solution convergence, the average boundary pressure will be close to the specified static exit pressure.

If the flow becomes locally supersonic, then the face pressure values are extrapolated from the interior cell pressure.

For the cold exit-pressure outlet pressure, the gauge pressure and backflow total temperature were varied depending on the experimental raw data [19], for example for cold mass fraction

of 0.2 the gauge static pressure was 19.99 kPa and backflow total temperature was 251.5 K. For backflow direction specification method used from neighboring cell.

For the hot exit-pressure outlet pressure, the gauge pressure was varied depending on the experimental raw data [19] but backflow total temperature was kept at 325 K, for example for cold mass fraction of 0.2 the gauge static pressure was 65.5 kPa. For backflow direction specification method used from neighboring cell.

For turbulence specification method used intensity and hydraulic diameter.

- **Axisymmetric flow with swirl**

The assumption of axisymmetry [13,14] implies that there are no circumferential gradients in the flow, there may still be non-zero swirl velocities. The flow is modeled as axisymmetric but includes the prediction of the circumferential velocity.

- **Tube walls**

No slip boundary conditions with adiabatic wall [13,14].

- **Turbulence model**

The results of the CFD model of the RHVT using the standard k-ε turbulence model showed the best agreement with the experimental results of Skye et al. [13,14]. Therefore, the standard k-ε turbulence model was selected to simulate the turbulence inside the VT in this study. For the near wall treatment, enhanced wall treatment was selected.

- **Model setup and convergence**

For solution method the best agreement with validated results were to use SIMPLE scheme for pressure-velocity coupling, The Spatial Discretization method is set to Second Order for all variables except for the pressure solver, the PRESTO method is chosen; the Fluent User's Guide suggests this method for strongly swirling flows.

For solution controls, under-relaxation factors were decreased to ensure reaching the convergence on all operating conditions.

For better convergence all residuals were adjusted to 1e-05 except for energy set to 1e-06.

To check the current numerical model beside validate the results against the experimental and previous CFD study [14], reversed flow through cold exit at low cold fraction for CFD current study was reviewed with every simulation to ensure following the flow behavior in other CFD studies [13,14] as shown below in "Fig. 13".

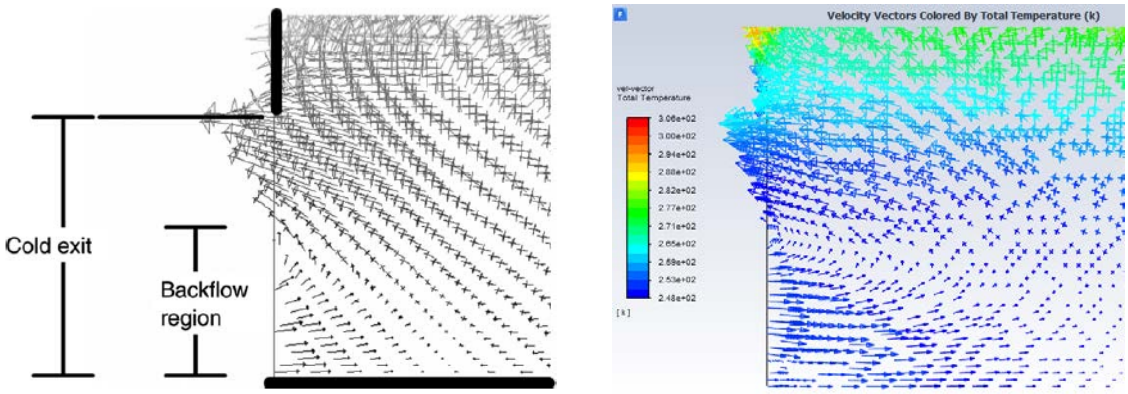

Figure 13: backflow through cold exit at low cold fraction of Skye et al. [14]in the left-hand side and current simulations at 0.2 cold mass fraction on the right-hand side.

Results of current study and validation with experimental data

The below "Fig. 14" shows the cold temperature separation for the current study which validated by experimental data of Skye et al. [14], also compared with CFD predicted values for their model. The current model shows agreement with experimental data especially in the cold mass fraction between 0.2 and 0.45 which could be for mesh enhancement over Skye et al. model [14] also could relate better convergence condition.

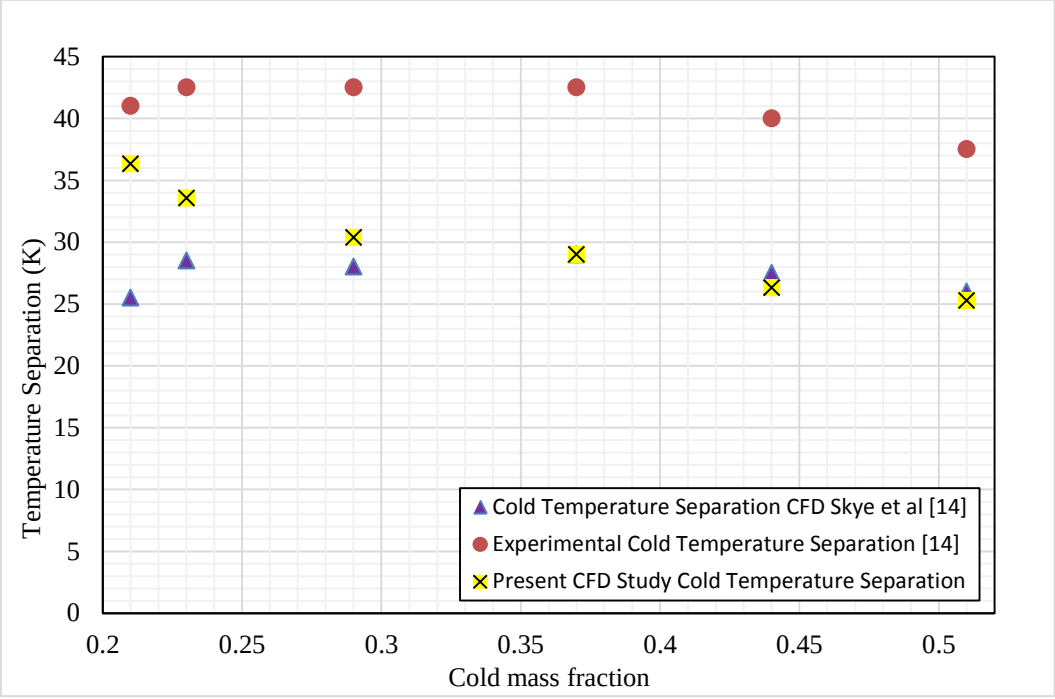

Figure 14: Cold Temperature Separation for current study, experimental data and previous CFD study values [14]

The below “Fig. 15” shows the hot temperature separation for the current study which validated by experimental data of Skye et al. [14], also compared with CFD predicted values for their model. The current model shows agreement with experimental data for the range of cold mass fraction between 0.35 to 0.52 which could be for mesh enhancement over Skye et al. model [14] also could relate better convergence condition.

For the range between 0.2 to 0.3 cold mass fraction the present model over simulated the values of temperature separation in opposite of Skye et al. model which is under estimated the values of experimental data but show lower difference.

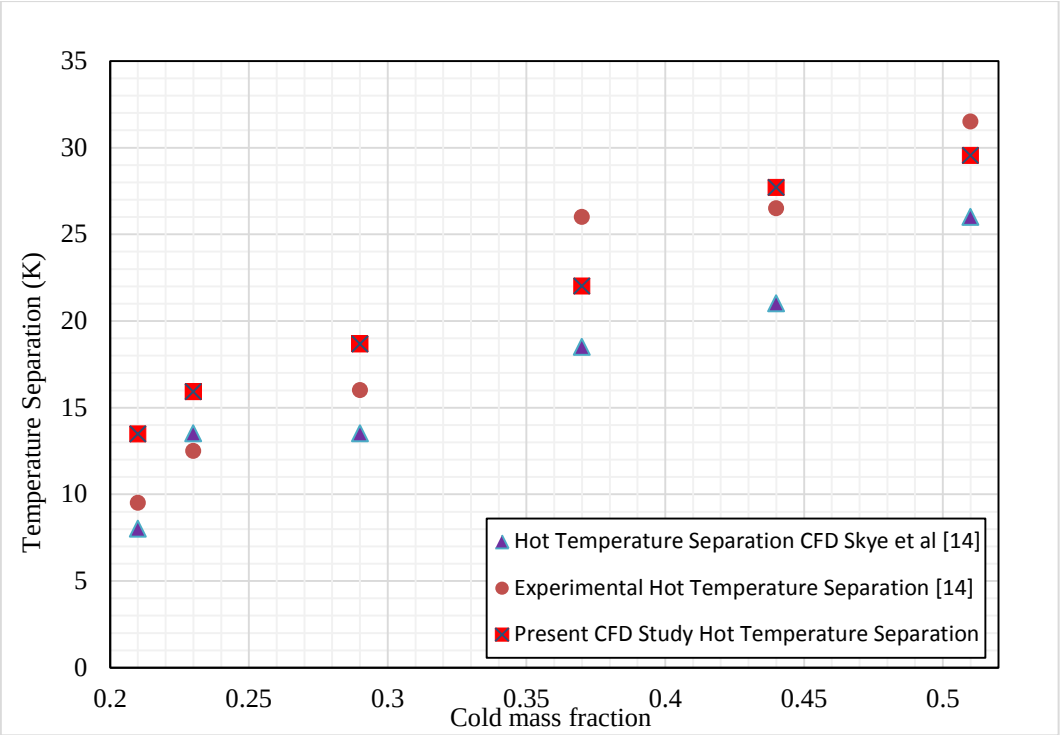

Figure 15: Hot Temperature Separation for current study, experimental data and previous CFD study values [14]

For “Fig. 16” which illustrates the cold power separation for the current study which validated by experimental data of Skye et al. [14], also compared with CFD predicted values for their model.

The current model shows better agreement with experimental data for the range of cold mass fraction between 0.2 to 0.45 which could be for mesh enhancement over Skye et al. model [14] also could relate better convergence condition.

For the range between 0.45 to 0.52 cold mass fraction the present model slightly under simulated the values of temperature separation in opposite of Skye et al. model.

For the last comparison in the results “Fig. 16” which demonstrates the hot power separation for the current study which validated by experimental data of Skye et al. [14], also compared with CFD predicted values for their model.

The current model shows better enhancement of matching with experimental data over the whole range of cold mass fraction over Skye et al. model [14] except for the first cold mass fraction.

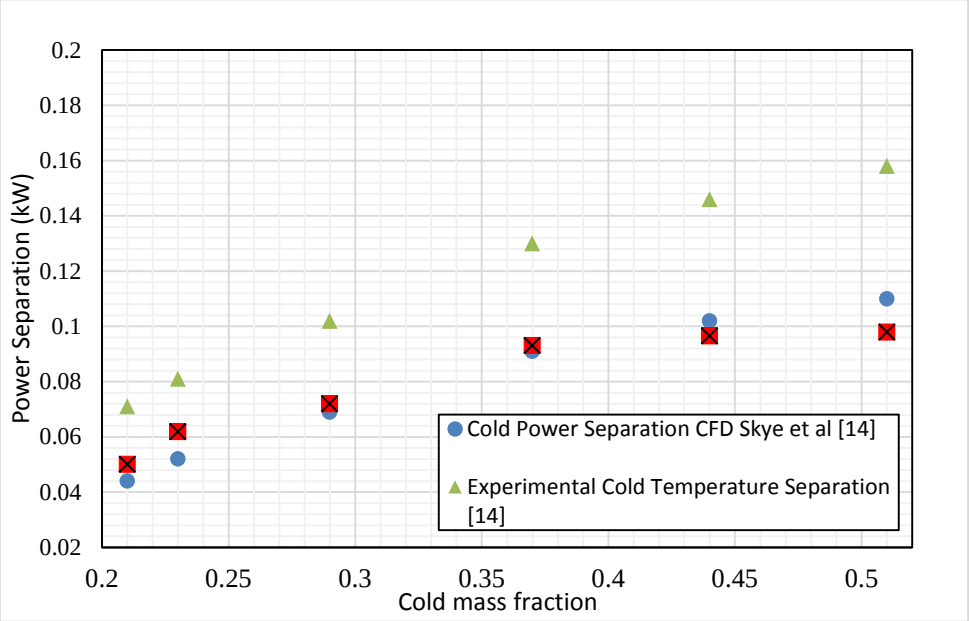

Figure 16: Cold power Separation for current study, experimental data and previous CFD study values [14]

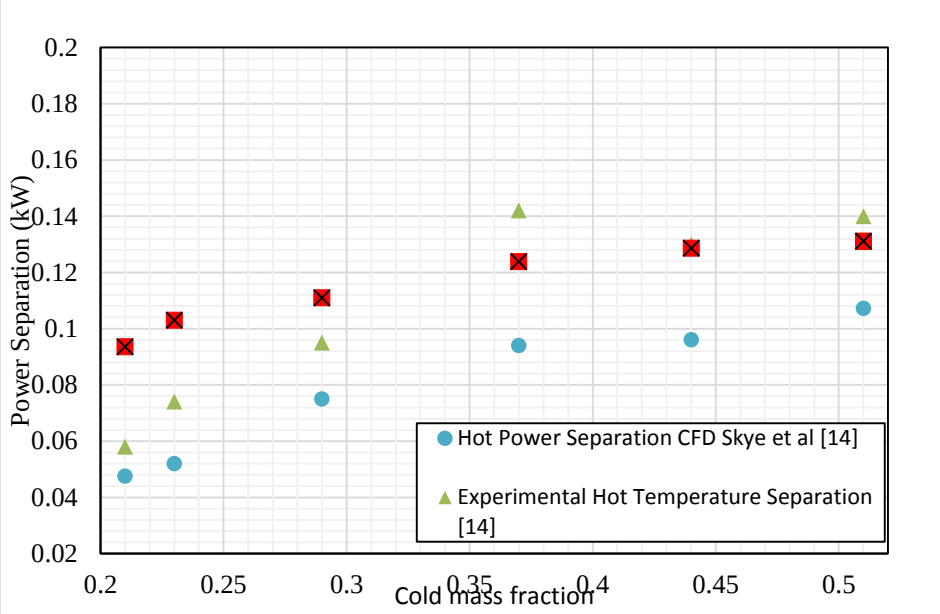

Figure 17: Hot power Separation for current study, experimental data and previous CFD study values [14]

Conclusion

The CFD model of the present study generally shows better agreement and enhanced values against the Skye et al [14] experimental data over their model within their published data. Due to the available and available experimental raw data the current study covers the cold mass fraction between 0.2 to 0.52 but in future the model should be tested against higher cold mass fractions up to 0.85 to evaluate the efficiency of the current CFD model.

Acknowledgment

I would like to express my deepest appreciation and gratitude to my friend Dr. Hesham Khalil for his patience and massive support during preparing the current paper.

References

[1]. Promvonge P, Eiamsa-ard S. Investigation on the vortex thermal separation in a vortex tube refrigerator. Science Asia. 2005;31(3):215-23.
[2]. Yilmaz M, Kaya ME, Karagoz S, Erdogan S. A review on design criteria for vortex tubes. Heat and mass transfer. 2009 Mar 1;45(5):613-32.
[3]. Xue Y, Arjomandi M, Kelso R. A critical review of temperature separation in a vortex tube. Experimental Thermal and Fluid Science. 2010 Nov 1;34(8):1367-74.
[4]. Sumanth R, Vishnu L, Prakash M. Fabrication and experimental analysis of a vortex tube. International Journal of Pure and Applied Mathematics. 2018;119(14):29-33.
[5]. Devade KD, Pise A. Parametric Review of Ranque-Hilsch Vortex Tube. American Journal of Heat and Mass Transfer. 2017;4(3):115-45.
[6]. Celik A, Yilmaz M, Kaya M, Karagoz S. The experimental investigation and thermodynamic analysis of vortex tubes. Heat and Mass Transfer. 2017 Feb 1;53(2):395-405.
[7]. Sahu R, Bhadoria R, Patel D. Performance analysis of a vortex tube by using compressed air. Int J Sci Eng Res. 2012 Sep;3(9).
[8]. Thakare HR, Patil YR, Parekh AD. A review of computational studies of temperature separation mechanism in vortex tube. Bonfring international journal of Industrial engineering and management science. 2013 Jun;3(2):74-80.
[9]. Thakare HR, Patil YR, Parekh AD. A review of computational studies of temperature separation mechanism in vortex tube. Bonfring international journal of Industrial engineering and management science. 2013 Jun;3(2):74-80.
[10]. Eiamsa-ard S, Promvonge P. Numerical investigation of the thermal separation in a Ranque–Hilsch vortex tube. International Journal of Heat and Mass Transfer. 2007 Mar 1;50(5-6):821-32.
[11]. Xue Y, Arjomandi M, Kelso R. A critical review of temperature separation in a vortex tube. Experimental Thermal and Fluid Science. 2010 Nov 1;34(8):1367-74.
[12]. Yun J, Kim Y, Yu S. Feasibility study of carbon dioxide separation from gas mixture by vortex tube. International Journal of Heat and Mass Transfer. 2018 Nov 1;126:353-61.

[13]. Kandil HA, Abdelghany ST. Computational investigation of different effects on the performance of the Ranque–Hilsch vortex tube. Energy. 2015 May 1;84:207-18.

[14]. Skye HM, Nellis GF, Klein SA. Comparison of CFD analysis to empirical data in a commercial vortex tube. International journal of refrigeration. 2006 Jan 1;29(1):71-80.

[15]. Sahu RA, Bhadoria Ro, Patel DE. Performance Analysis of a Vortex Tube by using Compressed Air. International Journal of Scientific & Engineering Research. 2012 Sep;3(9):1-7.

[16]. Maheswaran A, Purusothaman S, Shravanth BC. Design Of Vortex Tube And Analysis Of Its Flow Characteristics. International Journal of Engineering and Techniques. 2018 Oct; 4(5):45-51.

[17]. Kurosaka M. Acoustic streaming in swirling flow and the RanqueeHilsch (vortex-tube) effect. J Fluid Mech 1982;12(4):39-72.

[18]. Kazantseva OV, Piralishvili Sh A, Fuzeeva AA. Numerical simulation of swirling flows in vortex tubes. High Temp 2005;43(4):08-13.

[19]. H.M. Skye, Comparison of CFD analysis to empirical data in a commercial vortex tube. BS Thesis. Mechanical Engineering Department, University of Wisconsin, Madison; 2005.